An ancient lysozyme in placozoans participates in acidic extracellular digestion

Henry Berndt[1], Igor Duarte[1], Urska Repnik[2], Michel Struwe[1], Mohammad Abukhalaf[3], Axel Scheidig[1], Andreas Tholey[3], Harald Gruber-Vodicka[1,*] & Matthias Leippe[1,*]

1 Zoological Institute, Kiel University, Kiel, Germany

2 Central Microscopy, Kiel University, Kiel Germany

3 Proteomics & Bioanalytics, Institute for Experimental Medicine, Kiel University, Kiel, Germany

Lysozymes are an essential part of immunity and nutrition in metazoans, degrading bacterial cell walls via the hydrolysis of peptidoglycan. Although various lysozymes have been reported for higher animals, the origin of animal lysozymes remains elusive as they seem to be lacking in all early branching phyla. In this study, we investigated a putative goose-type lysozyme (PLys, glycoside hydrolase family 23, GH23) of the placozoan Trichoplax sp. H2. We show that PLys is highly active and produced in gland cells of the ventral epithelium. PLys contains a protective and non-conserved cysteine-rich domain N-terminal of the conserved GH23 lysozyme domain. A truncation of this N-terminal domain in the maturation process of PLys leads to a drastic increase in enzymatic activity at the cost of stability. As the lysozyme is most active under acidic conditions, we investigated the pH trajectories during extracellular digestion *in situ*. Using a pH-senstive fluorescence reporter, we show that *Trichoplax* sp. H2 acidifies its temporary feeding grooves pulsatively during digestive events close to the optimum pH for PLys activity. To elucidate the evolutionary origin of the metazoan GH23 lysozyme family, we applied a structure-based phylogenetics approach to show that the metazoan g-type GH23 lysozymes originated from a horizontal gene transfer event from bacteria to an early pre-bilaterian ancestor. GH23 lysozymes have then been retained and expanded in many phyla, including Porifera, Cnidaria, Placozoa and chordates, acting as first animal lysozyme and a key component in the antibacterial arsenal since early animal evolution.

*: Corresponding authors e-mail addresses – mleippe@zoologie.uni-kiel.de , hgrubervodicka@zoologie.uni-kiel.de

Main:

Animals are always associated and interacting with bacteria. These interactions can range from beneficial mutualism between host and microbe to one side taking advantage, e. g. bacterial pathogens or bacterivorous animals (1). For killing and digestion of bacteria, animals feature a variety of molecular processes and effector proteins. A key group of such antibacterial proteins are lysozymes, glycoside hydrolases (GHs) that attack the peptidoglycan layer by cleaving the β-1,4-glycosidic bond between its main building blocks N-acetylmuramic acid (MurNAc) and N-acetylglucosamine (GlcNAc). Lysozymes have been traditionally grouped into different classes, named after the organisms in which they were first discovered (2). A more consistent naming convention for enzymes with a glycoside hydrolase activity categorizes them into families based on their fold and substrate specificity. For example, goose-type (g-type) lysozymes, first discovered in the egg white of the graylag goose *Anser anser* and found later in many vertebrates, belong to the glycoside hydrolase family 23 (GH23), together with bacterial lytic transglycosylases (3).

Lysozymes appear to be very unevenly distributed in the animal tree of life, with most early branching clades such as Ctenophora and Cnidaria apparently lacking *bona fide* lysozymes (2). While protostomian invertebrates as well as early branching deuterostomes such as echinoderms predominantly feature invertebrate-type (i-type) lysozymes of GH22i, chordates primarily possess g-type (GH23) and chicken-type (c-type) lysozymes (GH22c) (2,4). Sparse reports of c-type lysozymes in Arthropoda and g-type lysozymes in mollusks, however, challenge the evolutionary argument that these two lysozyme families are limited to Chordata (2). In addition, a short report about a putative g-type in placozoans, provisionally named PLys, suggests that the evolution of major lysozyme groups in animals was not a relatively late innovation in the lineages leading to bilaterians and then chordates (5). The existence of a potential g-type lysozyme in some of arguably the simplest metazoan animals points instead to a much earlier occurrence and diversification of lysozymes in the animal tree of life (ATL). The position of Placozoa in the ATL is under ongoing discussion, but recent bioinformatic

65 analyses consistently place placozoans among the pre-bilaterian lineages and as the
66 sister taxon to the clade formed by Cnidaria and Bilateria (6,7). With such an interesting
67 position in animal phylogeny, placozoans are increasingly used as a model organism to
68 study the origin of multicellularity, developmental biology, and neurophysiology (8–10).
69 As millimeter-sized and disk-shaped grazers of marine biofilms, placozoans continually
70 interact with bacteria, and also harbor endosymbiotic bacteria in a cell-type specific
71 symbiosis (11,12). The basic body plan of the placozoans is very simple and consists of
72 three layers. The ventral columnar epithelium has a mainly digestive function, whereas a
73 thin dorsal epithelium has primarily a barrier function. A densely packed mesenchyme-
74 like layer consists of fiber-cells, which form many cell-to-cell connections with other cell
75 types in both epithelia (13). In addition, fiber cells contain endosymbiotic bacteria, and
76 have been highlighted as central immune cells in placozoa, as they are the only cells
77 capable of phagocytosis and apoptosis (11,14). During feeding, placozoa form a
78 temporary gastric cavity between the ventral epithelium and the substrate, into which
79 gland cells and lipophilic cells secrete digestive enzymes (15). Comparative single-cell
80 transcriptomics data of diverse placozoan lineages showed *plys* to be almost exclusively
81 transcribed in gland cells of the ventral epithelium, from where PLys could be secreted
82 into the gastric cavity (6).
83
84 To elucidate the role of PLys in *Trichoplax* sp., we identified the natural proteoforms of
85 the lysozyme, produced the two lysozyme variants recombinantly, characterized them *in*
86 *vitro* and determined their cellular distribution in whole animals. Using evolutionary
87 analyses, we show that the highly active lysozyme PLys represents a broad radiation of
88 g-type lysozymes across the animal tree of life that arguably were among the earliest
89 antibacterial effectors in metazoan evolution.
90 **Results and Discussion:**
91 **Identification and localization of native placozoan lysozyme**
92 As a putative g-type lysozyme has been reported for placozoans (PLys) (5) and the
93 corresponding orthologous gene is transcribed across different placozoan species (Fig.
94 S1), we screened for the activity of lysozymes using placozoan total protein extract from

95 *Trichoplax* sp. H2. On a lysoplate, placozoan total protein extract in two concentrations
96 (0.24 mg/mL and 1.24 mg/mL) produced zones of lysis after 24 h (Fig. 1A). Following this
97 first indication of lysozyme activity, we validated the identity of the potential lysozymes
98 by mass spectrometry and Western blotting of a reversed-phase chromatography
99 fractionated *Trichoplax* proteome. The Western blot revealed two protein double bands,
100 which correspond to molecular masses of about 30 kDa and 20 kDa, matching the two
101 proteoforms previously mentioned by Bam and Nakano (Fig. S2) (5). We therefore used
102 fractions with the strongest signals in the western blot for mass spectrometry to
103 characterize these two potential proteoforms in a combination of proteomic analyses of
104 intact proteins without further processing (top-down) and of proteolytically generated
105 protein fragments (peptide-based; bottom-up). In top-down experiments, the most
106 abundant proteoform was lacking the N-terminus and started at amino acid residue S100
107 (Fig. 1B). Based on the structural model of the full length PLys predicted by ColabFold,
108 the N-terminal domain that is missing in this most abundant proteoform consists of two
109 repeated beta-sheets, is stabilized by 6 disulphide bonds, and is connected to the active
110 g-type lysozyme domain by a loop. N-terminomics (Bottom-up proteomics) experiments
111 detected peptides specific to this N-terminal domain of the full-length PLys. The N-
112 terminus (S100) of the shorter form of PLys is located in the connective loop region
113 between the N-terminal domain and the lysozyme domain (Fig. 1C), which likely
114 constitutes a cleavage site for specific proteolytic processing during protein maturation
115 (limited proteolysis). We therefore differentiate between the truncated and presumably
116 mature PLys (mPLys) and the full-length precursor PLys (pPLys) in the later experiments.
117
118

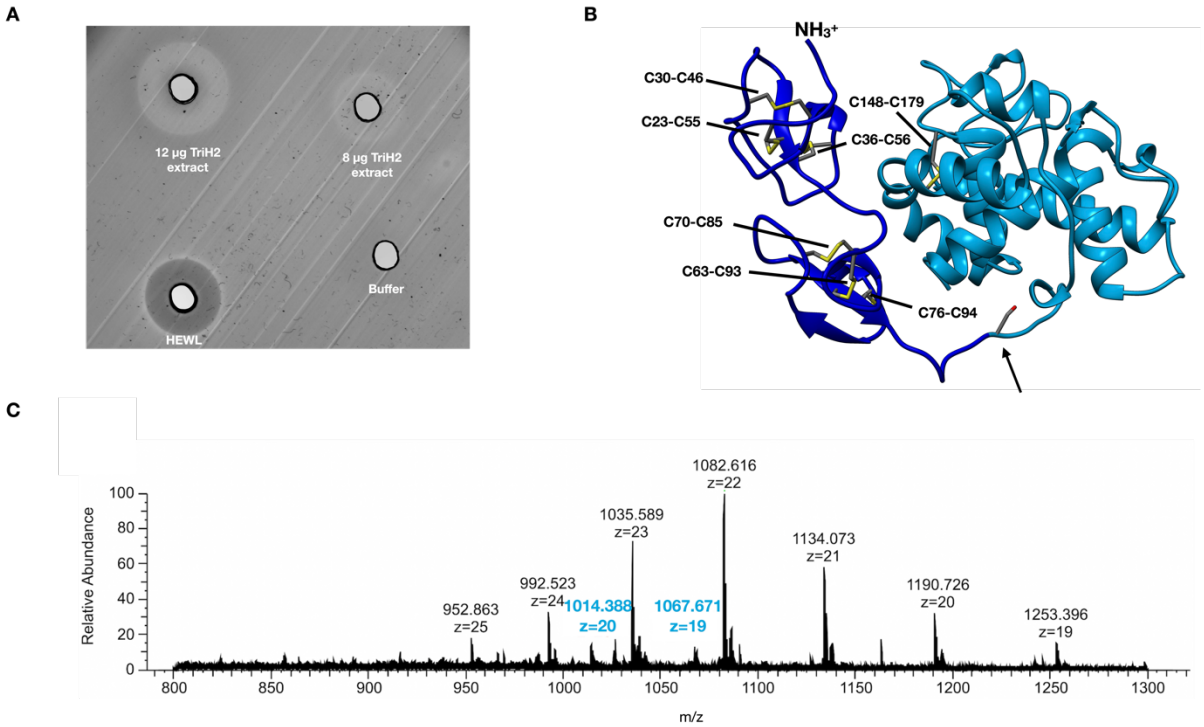

Figure 1: PLys is an active lysozyme with a truncated mature proteoform. A): Lysoplate assay with 8 µg and 12 µg total protein of raw *Trichoplax* sp. H2 protein extract, 20 µg hen egg white lysozyme (HEWL), and lysis buffer. **B)**: Structure model of PLys as ribbon diagram. The backbone of the mature proteoform of PLys is colored in light blue, while the cysteine-rich N-terminal domain is colored in dark blue. Cysteine residues forming disulphide bonds are highlighted and annotated. An arrow marks S100, the apparent N-terminus of the physiologically mature proteoform. **C**): Representative mass spectrum of the top-down proteomics experiment with the identified mature PLys proteoform with charge states z=19 and z=20.

Following the identification of the two forms of PLys in the *Trichoplax* sp. H2, we applied immunohistochemical labeling of PLys for cellular localization of the enzyme. Lysozymes are usually either secreted for extracellular lysis of bacteria or act on phagocytosed bacteria in phagolysosomes (2). As fiber cells have been indicated as the only cell type in *Trichoplax* capable of engulfing bacteria (14), we predicted that PLys is detectable either in lysosomes of fiber cells or in exocytotic vesicles of secretory cells of the ventral

136 epithelium (gland cells or lipophilic cells). In general, placozoans feature an upper (dorsal)
137 epithelium (d, Fig. 2A), made up by dorsal epithelial cells, and a lower (ventral) epithelium
138 (v, Fig. 2A) which is populated by ventral epithelial cells, gland cells, and lipophilic cells
139 (13,16). Lipophilic cells are characterized by large vesicles close to their apical
140 membrane which are stainable using lipophilic and acidophilic dyes (15). A mucus
141 secreting subtype of gland cells shows high abundance in the peripheral region of the
142 ventral epithelium that is stainable with wheat germ agglutinin (WGA) (16). The region
143 between the epithelia is mostly covered by fiber cells and to a smaller degree by gravity-
144 sensing crystals cells (13,14). The signal of the PLys-specific polyclonal antibodies was
145 present across the animal (Fig. 2B) and localized mostly to cells in the ventral epithelium
146 (Fig. 2C). We also observed labeling in traces of mucus the animal left behind, which is
147 another indicator for secretion of the enzyme (Fig. 2B). Additionally, we occasionally
148 observed accumulation of signals between ventral and dorsal epithelium that could
149 origin from fiber cells. Our antibody staining is consistent with single-cell expression data
150 demonstrating *plys* expression predominantly in gland cells (6). Given the inconsistent
151 anti-PLys-signal in fiber cells, it remains unclear, whether fiber cells are able to import
152 gland-cell secreted lysozyme, or if the synthesis of lysozyme in fiber cells is inducible by
153 bacterial components. While the genome of the closely related *Trichoplax adhaerens*
154 appears to code for a high variety of scavenger receptors and reveals parts of Toll-like
155 and NOD-like signaling pathways that may detect bacterial molecular patterns, complete
156 signaling pathways from receptors to transcription factors that induce and regulate the
157 synthesis of innate immunity factors such as PLys have yet to be identified (17).

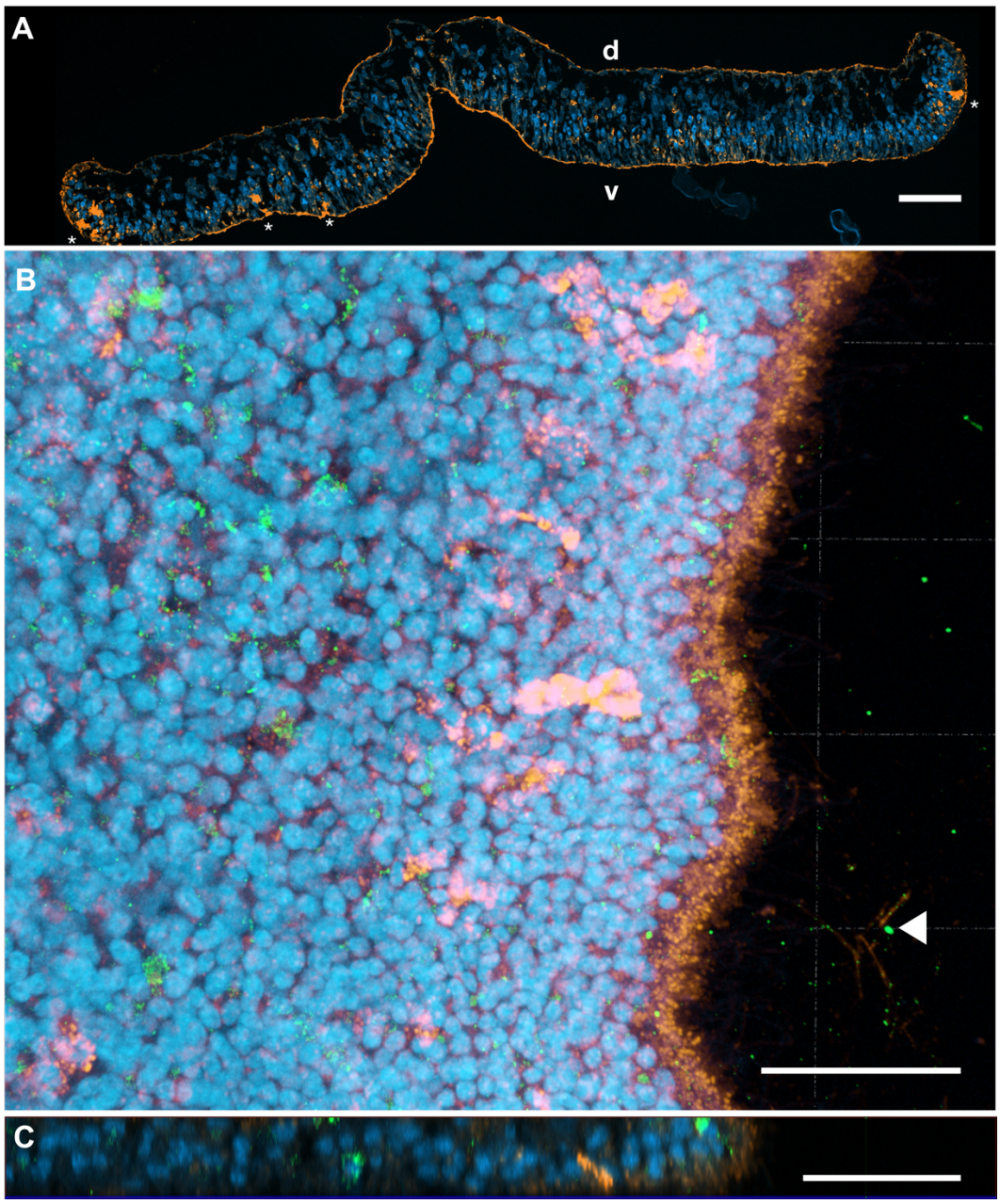

Figure 2: PLys is abundant in gland cells of the ventral epithelium and detectable in secreted mucus. A) Cross-section of a resin-embedded *Trichoplax* sp. H2 individual, highlighting dorsal (d) and ventral (v) epithelia as well as mucus-secreting gland cells (asterisks). DAPI = blue, Wheat-germ agglutinin (WGA) = orange. **B)** Dorsal to ventral view on a 3D-projection of a Z-stack of a *Trichoplax*. sp. H2 wholemount stained with anti-PLys (green), WGA (orange) and DAPI (blue). Co-labeling of mucus and PLys in trails of the animal is indicated with an arrowhead. **C**) Partial 2D-orthographic projection (YZ) of the Z-stack shown in Fig. 2B. Scale bars correspond to 20 µm.

167 **PLys proteoforms show highest lysozyme activity under acidic conditions**
168 Given the contrasting domain architecture of the two forms of PLys, we wanted to
169 understand the role of the cleaved N-terminal domain that characterizes pPLys. We
170 therefore heterologously expressed both pPLys and an mPLys variant recombinantly,
171 where mPLys consisted of the g-type lysozyme domain starting at amino position 112
172 (M112) of pPLys (mPLys_M112). A comparison of pPLys and mPLys_M112 lysozyme
173 activity at room temperature against freeze-dried *Micrococcus lysodeikticus* revealed
174 high specific activities for both variants compared to hen egg white lysozyme (HEWL) at
175 pH 5.0 (21°C; pPLys = 9 U/pmol; mPLys_M112 = 11 U/pmol; HEWL = 0.5 U/pmol) (Fig.
176 3B). Both variants had maximum activity under low ionic strength (<50 mM) and at a pH
177 between 5.0 and 5.5 (Fig. 3C-D). The specific activity of mPLys_M112 at its pH optimum
178 (pH 5.5) was three times higher than that of pPLys at its respective optimum (pH 5.0)
179 (Fig. 3E). We also tested the bacteriolytic activity of both proteoforms against viable
180 *Bacillus subtilis* and *Escherichia coli* D31 by assessing the dose-dependent increase in
181 fluorescence of a membrane-impermeable DNA-binding dye (Fig. 3F-G). Both PLys
182 variants showed high activity against *B. subtilis* with LD50 values of 100 nM
183 (mPLys_M112) and 130 nM (pPLys). However, we found no lytic activity against the
184 tested gram-negative *E. coli* strain. The lack of activity against gram-negative bacteria is
185 contrary to the results of PLys by Bam and Nakano (5) but consistent with most
186 metazoan lysozymes being inactive towards gram-negative bacteria (2).
187
188
189
190
191
192
193
194
195

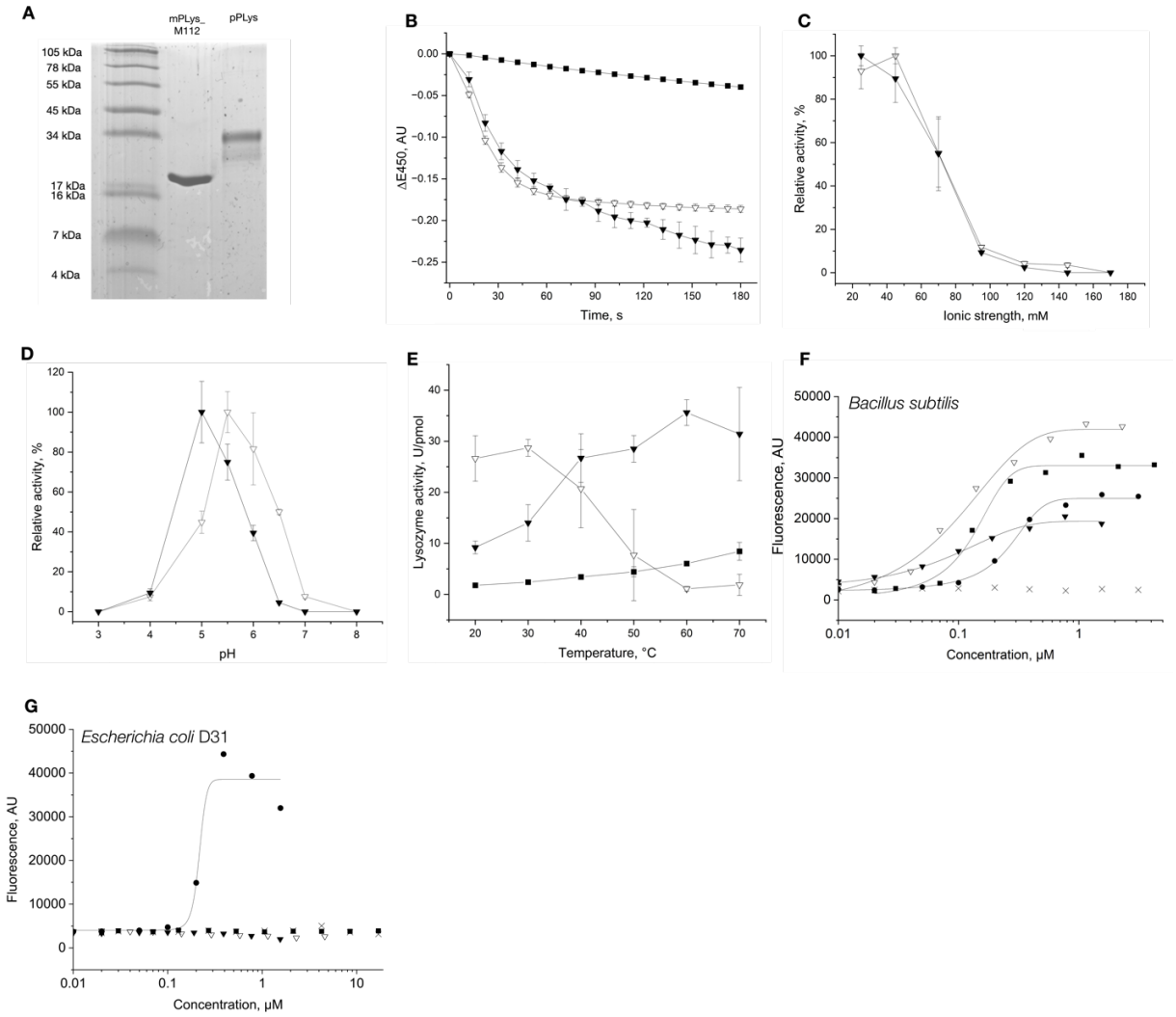

Figure 3: PLys is a potent lysozyme under acidic conditions. A): SDS-PAGE gel of purified recombinant mPLys_M112 and pPLys. The molecular mass standard is indicated on the left and marked with the associated molecular masses in kDa. **B**): Lysozyme assay of 32 pmol pPLys, 32 pmol mPLys_M112, and 32 pmol HEWL at pH 5.0. Reaction buffer consisted of 20 mM sodium acetate, pH 5.0 (I = 13 mM). **C,D**): Dependency of lysozyme activity of pPLys and mPLys_M112 on ionic strength (C) and pH (D) at room temperature. **E**): Lysozyme activity of pPLys, mPLys_M112 and HEWL at different temperatures. All measurements were performed in triplicates. **F,G**): Bacterial lysis assay against *B. subtilis* (F) and *E. coli* D31 (G) using a membrane-impermeable dye (SYTOX Green). Fluorescence indicates lysis of cells. Sigmoidal functions were fitted to the dose response curves. mPLys_M112: open triangles, pPLys: closed triangles, HEWL: closed squares, Melittin: closed circles, buffer control: crosses.

208 **pPLys has a much higher optimal temperature and is active at a broader range of**
209 **temperatures than mPLys**
210 Since the N-terminal domain of PLys is stabilized by six disulphide bonds, we
211 hypothesized that enzyme activity of the proteoforms could strongly deviate under
212 temperature increase. Our screens across a broad temperature range indeed revealed
213 that the specific lysozyme activity of pPLys increased until 60 °C and virtually stayed at
214 this level at 70 °C, while mPLys_M112 activity peaked at 30 °C and decreased
215 proportional to the increase in temperature (Fig. 3E). Following the strong difference in
216 heat tolerance, we assessed the denaturing dynamics (melting temperatures) for both
217 variants. mPLys_M112 denatured between 25 °C and 35 °C, whereas pPLys denatured
218 between 50 °C and 60 °C, consistent with their temperature-activity profiles (Fig. S4).
219 Overall, the pPLys N-terminal domain appears to have a strong stabilizing effect under
220 physiologically relevant temperatures, at the cost of activity. G-type lysozymes typically
221 contain two disulphide bonds, whereas the PLys lysozyme domain only contains one
222 (18). The increased structural flexibility introduced by the loss of a disulphide bond could
223 explain both increased activity at low temperatures due to an induced-fit type of
224 substrate binding and decreased stability at higher temperatures (19). In pPLys, the
225 cysteine-rich N-terminal domain may compensate for the loss of the disulphide bond
226 and stabilize the protein until maturation to prevent a fast physiological turn-over. We
227 hypothesize that *Trichoplax* uses this trade-off between stability and activity by cleaving
228 the N-terminus from pPLys before secretion. The cysteine-rich repeats (CRRs) which
229 constitute the N-terminus are widely distributed across eukaryotes and were linked to
230 horizontal gene transfer (HGT) events from prokaryotes (20,21). These CRRs are
231 abundant in proteins associated with antimicrobial activity, in which one or multiple
232 CRRs constitute the N-terminus Temperature-dependent activity studies on entire and
233 truncated variants of other proteins with this N-terminal CRR domain structure may
234 elucidate whether the stabilizing effect promotes the selection of this domain
235 architecture and hence has been conserved.
236
237

238 **Trichoplax sp. H2 acidifies its temporary feeding grooves for extracellular digestion**
239 Placozoans form a temporary gastric cavity (feeding groove) only when moving onto their
240 feeding substrate (22). Lipophilic cells and gland cells in the ventral epithelium
241 subsequently show a secretory burst of vesicles, which releases digestive enzymes. In
242 a preliminary study, Mayorova et al. investigated the same 'gland cell' annotated meta-
243 cells that are the main expressing cells of *plys* in *Trichoplax* sp. H2. For trypsin, which is
244 also predominantly produced by this cell type, they showed extracellular activity in
245 feeding grooves within digestive events (23). This finding supports our localization of
246 PLys to secretory gland cells and implies that PLys also acts in temporary feeding
247 grooves. Due to the strong dependency of PLys activity on acidic conditions, we
248 hypothesized that placozoans can acidify their feeding grooves despite their temporary
249 nature. To assess the pH during extracellular digestion events, we offered *Trichoplax* sp.
250 H2 zymosan-particles (inactivated yeasts) coupled to a pH-sensitive fluorescent dye (Fig.
251 S5-6) and recorded digestion events in time series (Fig. 4A). While the pH in the feeding
252 grooves initially corresponded to the pH of the surrounding sea water (pH 8.5), we
253 observed spontaneous drops of pH. The pH stayed acidic for multiple tens of seconds
254 and slowly equilibrated back to the initial pH (Fig. S7-8). Over multiple replications of the
255 experiment, we observed an average minimum pH of 6.0 (Fig. 4B), which is close to the
256 activity optimum of mPLys (Fig. 3D). Previous studies on the feeding behavior of
257 *Trichoplax* sp. indicated gland cells and lipophilic cells as primary secretory cells in the
258 feeding process, in which gland cells largely contribute digestive enzymes and lipophilic
259 cells may contribute to the acidification with a secretory burst of vesicles stainable with
260 acidophilic dyes (15). Release of the acidic content of these vesicles in vast amounts
261 may facilitate acidification of the gastric cavity, potentially down to the physiologically
262 optimal conditions for the activity of PLys and other digestive enzymes. Further
263 enzymological characterization of other digestive enzymes of *Trichoplax* spp. may
264 elucidate whether all extracellular digestive processes in placozoans are adapted to
265 acidic conditions.
266
267

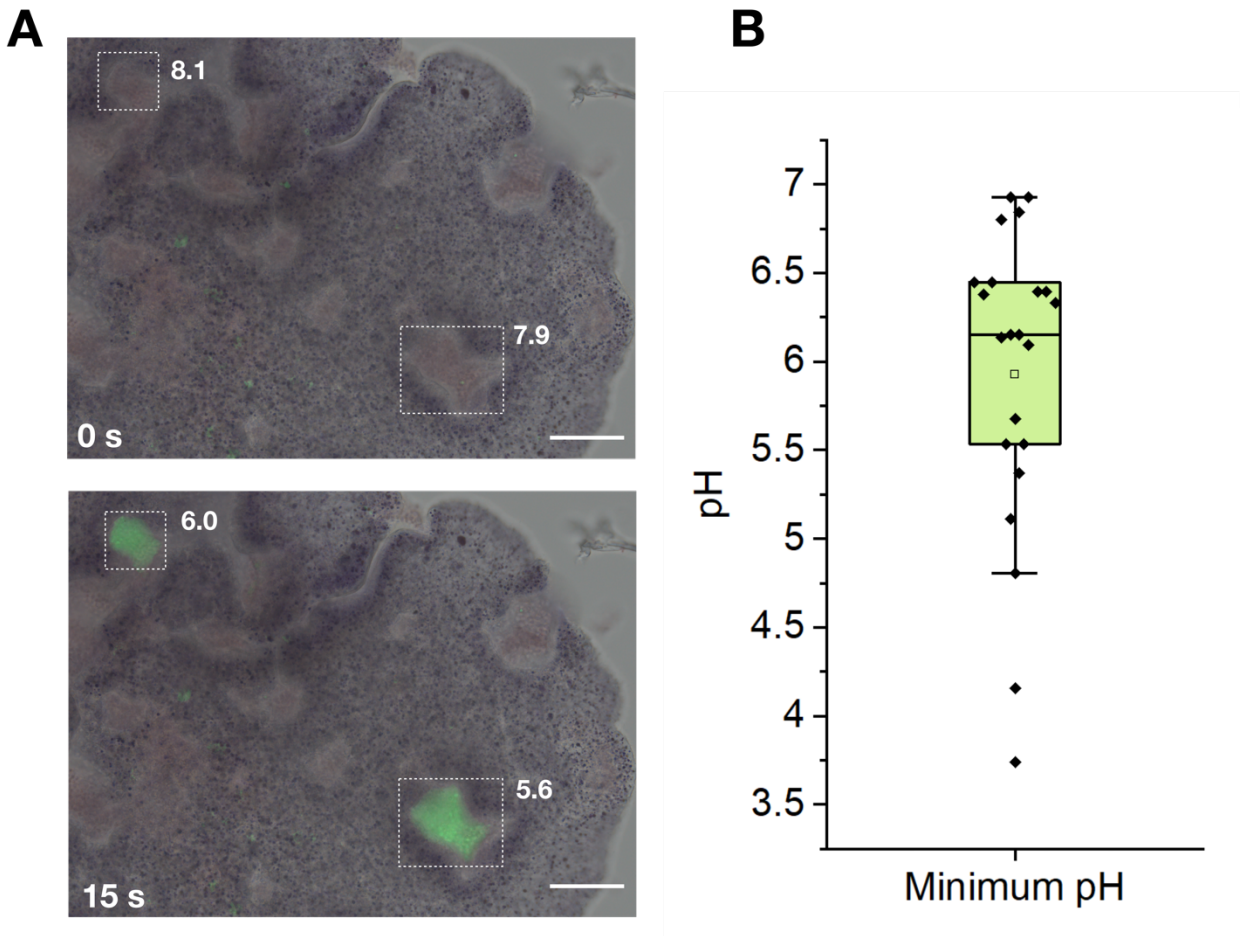

Figure 4: Placozoa acidify their temporary feeding groove pulsatively. A): Merged micrographs in brightfield and green-epifluorescence mode of *Trichoplax* sp. H2 feeding on zymosan particles coated with a pH-sensitive dye after 0 s and 15 s. Two feeding grooves are highlighted by dotted lines. The corresponding pH is presented next to the grooves. Scale bars: 50 µm. **B**): Box plot of the minimum recorded pH (closed diamonds) of digestive events (n=22). The open square shows the mean, the horizontal line represents the median.

282 However, how placozoans lower ionic strength to less than 10% of the surrounding
283 seawater medium remains enigmatic. One possible mechanism may involve the mucus,
284 which is secreted by gland cells in the ventral epithelium. Mucins, the main component
285 of metazoan mucus, are complex proteoglycans which often carry negatively charged
286 building blocks such as carboxy groups, sulfate groups, or sialic acid residues (24). It
287 has already been shown that the negatively charged components of mucins can bind
288 sodium ions and their hydrate shells, causing swelling of the mucus and formation of a
289 biogel (25). Similarly, in placozoans, the nascent mucus in the gastric cavity could
290 potentially take up inorganic cation species from the seawater medium, which is
291 dominated by sodium ions, and lead to a decrease of ionic strength in the aqueous phase
292 inside the gastric cavity. Depending on the pH inside the mucus-loaded exocytotic
293 vesicles of the gland cells, carboxy-groups in the mucus may be initially protonated and
294 lead to proton-sodium exchange between mucus and seawater after secretion, which
295 would also cause a decrease of pH in the gastric cavity. Chemical analysis of placozoan
296 mucus would be necessary to characterize the molecular function of mucus in these
297 early branching metazoans.
298
299 **G-type lysozymes presumably originated from an ancient lateral gene transfer**
300 Placozoa are one of the earliest branching animal phyla. As they feature the PLys
301 lysozyme of the GH23 family only, this lysozyme family may have been the earliest in
302 metazoan phylogeny. As the GH23 family also comprises bacterial lytic
303 transglycosylases, this is particularly intriguing. Bacterial lytic transglycosylases also act
304 on peptidoglycan but catalyze the formation of 1,6-anhydromuramyl residues through
305 an intramolecular nucleophilic attack instead of hydrolysis. They are housekeeping
306 genes important for the biosynthesis and turnover of the bacterial cell wall (3). To
307 elucidate the evolution of metazoan g-type lysozymes and to investigate the relationship
308 between GH23 lysozymes and bacterial lytic transglycosylases, we hence constructed
309 a database of all GH23_I members including a set of closely related bacterial lytic
310 transglycosylases that possess the specific sequence motif of the GH23_I. Amino acid
311 sequences were obtained from the carbohydrate active enzyme (CAZY) database,

BLAST searches with PLys against nr, and the manual addition of a curated group of GH23_I orthologs detected in metazoan genome assemblies without previously annotated g-type lysozymes (26) (Fig. 5 and S9). We also included sequences of myxobacterial GH23 orthologues, which have been proposed as indicators of a horizontal gene transfer (HGT) from myxobacteria to a metazoan ancestor in a parallel study (27).

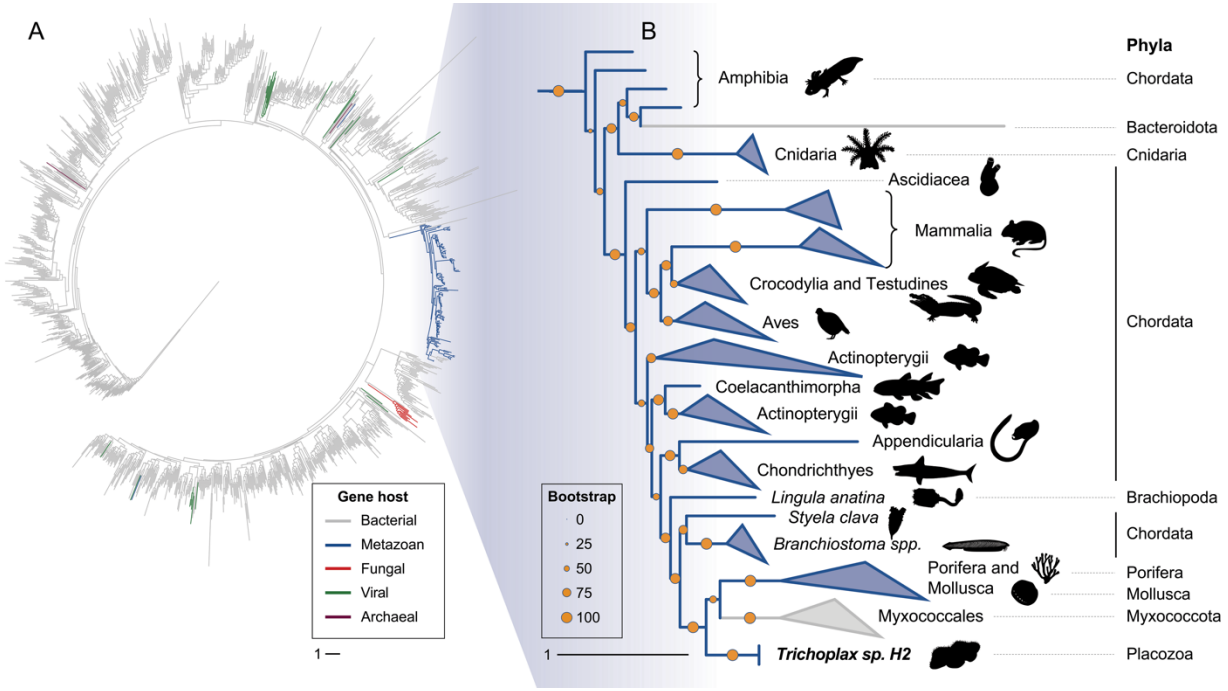

Figure 5: Metazoan g-type lysozymes cluster predominantly into a single clade and are present in six animal phyla. A) Phylogenetic tree of 1428 glycoside hydrolase family 23 sequences from all domains of life and **B**) expanded tree branch containing all metazoan sequences. Colors indicate host groups, orange dots show phylogenetic support (aLRT).

331 In our phylogenetic analysis, out of the 131 metazoan g-type lysozymes included in the
332 dataset, 129 clustered in a single clade (clade support: 99.3), which is nested inside the
333 bacterial lytic transglycosylases. Intriguingly, the manually added myxobacterial
334 orthologues clustered in a monophyletic clade which itself is nested inside the metazoan
335 GH23 lysozyme clade, while other myxobacterial GH23 orthologues annotated as
336 soluble lytic transglycosylases were placed within the bacterial sequence clades. We
337 therefore interpret the myxobacterial sequences clustering in the metazoan clade as
338 professional lysozymes and not lytic transglycosylases, also considering the predatory
339 bacterivorous lifestyle of myxobacteria (28). Additionally, the branch lengths between the
340 myxobacterial lysozymes and the next metazoan relatives are rather short compared to
341 the long branch separating the metazoan clade from the bacterial lytic transglycosylases,
342 which indicates a shorter time frame of molecular evolution. These results indicate the
343 myxobacterial GH23 lysozymes to have originated in a lateral gene transfer of a
344 metazoan GH23 lysozyme to a myxobacterial ancestor, while the metazoan GH23
345 lysozymes itself originated from a much older HGT of a bacterial lytic transglycosylase
346 to a metazoan ancestor. While the molecular evolution trajectory of most GH23 lysozyme
347 orthologues within the metazoan clade was consistent with the phylogenetic
348 relationships of the respective organisms, we occasionally observed the clustering of
349 orthologues from phylogenetically distant species. This could be due to gene duplication
350 and different evolutionary trajectories of the resulting paralogues or to the horizontal
351 gene transfer between different metazoan ancestors, which has been reported for a
352 subgroup of protostomian g-type lysozymes (27). The prevalence of g-type lysozymes
353 in all early branching animals (Porifera, Cnidaria and Placozoa) except Ctenophora
354 suggests that g-type lysozymes originated during early metazoan evolution. The g-type
355 lysozyme appears to be an innovation of the lineage split from ctenophores and would
356 support the hypothesis of ctenophores being a sister phylum to all other metazoans (29).
357 The gene was then lost in most of the Protostomia except mollusks and brachiopods,
358 while it was retained in most chordate lineages (Fig. 6).
359
360

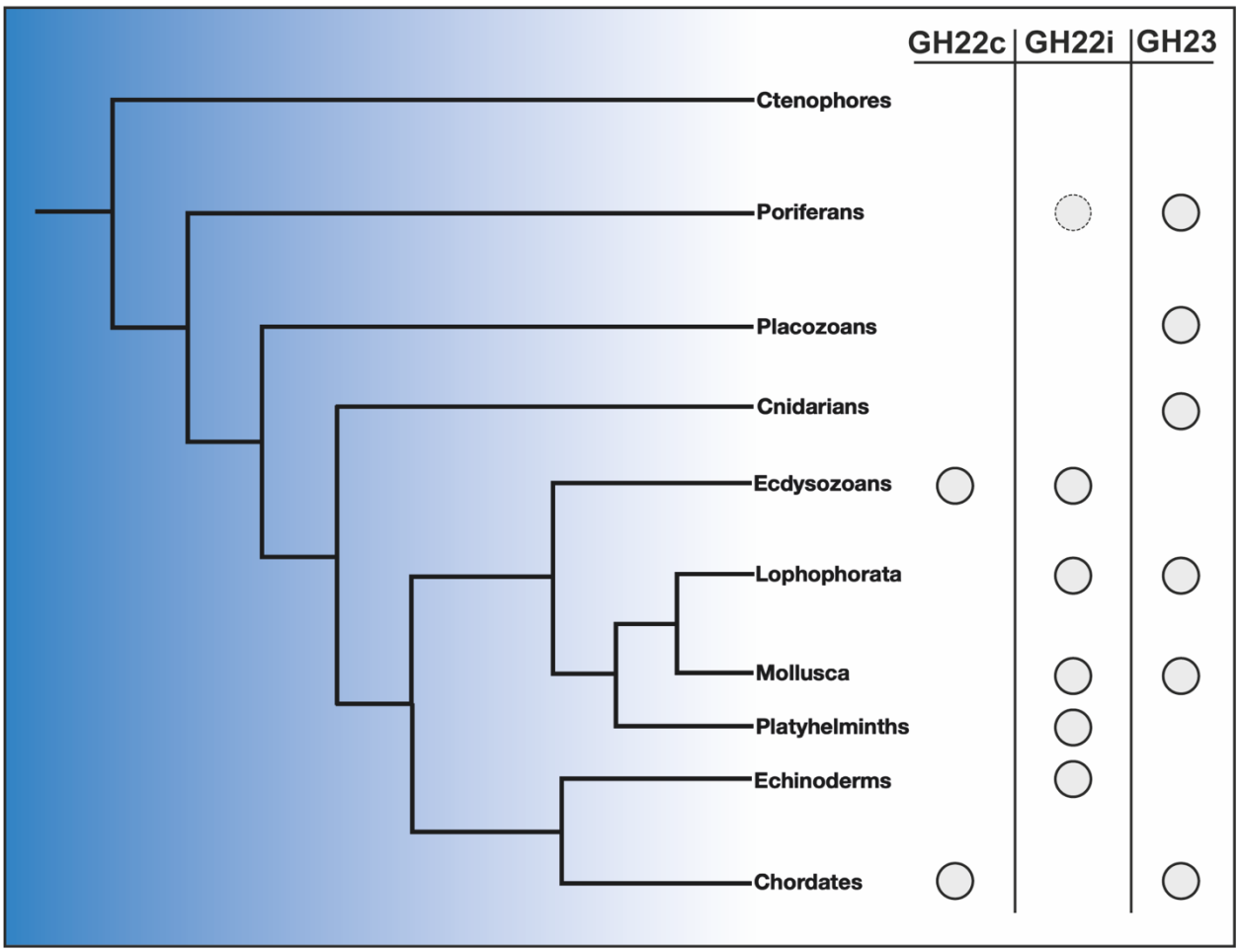

Figure 6: G-type lysozymes are widely distributed over the animal tree of life and the only lysozyme of early all early branching metazoans except ctenophores. Overview phylogram of metazoans according to Laumer et al. (7) that shows the distribution of the most abundant lysozyme families (closed circles). The status of lysozyme abundance is based on Callewaert and Michiels (2), Berndt et al. (30) and this study. As only one GH22i lysozyme has been reported for poriferans (31), the respective circle is dotted.

375
376 All early branching animals lack homologues of any other lysozyme subfamily, except a
377 description of an i-type lysozyme in the sponge *Suberites domuncula* (31). In a previous
378 phylogenetic analysis of i-type lysozymes, we showed the *Suberites* lysozyme to be
379 most similar to deuterostomian i-type lysozymes (30). As all other analyzed Porifera lack
380 i-type lysozymes, this could either be a contamination or a secondary acquisition of the
381 i-type lysozyme by an ancestor of *Suberites*. While all metazoan g-type lysozymes
382 cluster together and diverge from bacterial lytic transglycosylases, the exact relationship
383 between these ancient and very similar protein folds, which show low sequence identity
384 but a substantial structural conservation, are difficult to resolve from primary structure
385 analyses. Protein folds and structural sub-motifs of homologous proteins have been
386 shown to be more conserved than their amino acid sequences (32,33). Additionally, the
387 invention of fast and highly accurate protein prediction algorithms allow to generate
388 reliable protein structure models, which can be used for these deep evolutionary
389 analyses (34–36). We therefore used a tertiary-structure based phylogenetics approach
390 to reconstruct deeper relationships within the lysozyme superfamily and included c-type
391 and i-type lysozymes as well as the most closely related GH-families (1449 structures in
392 total) (4,36). The metazoan GH23 lysozyme branch separates from all other metazoan
393 lysozyme families and branches within clades of GH23 bacterial lytic transglycosylases,
394 while the metazoan lysozymes of the GH22i and GH22c subfamilies cluster together with
395 the phage-type lysozymes of the GH24 and GH46 (Fig. 7 and S11).
396
397
398
399
400
401
402
403
404

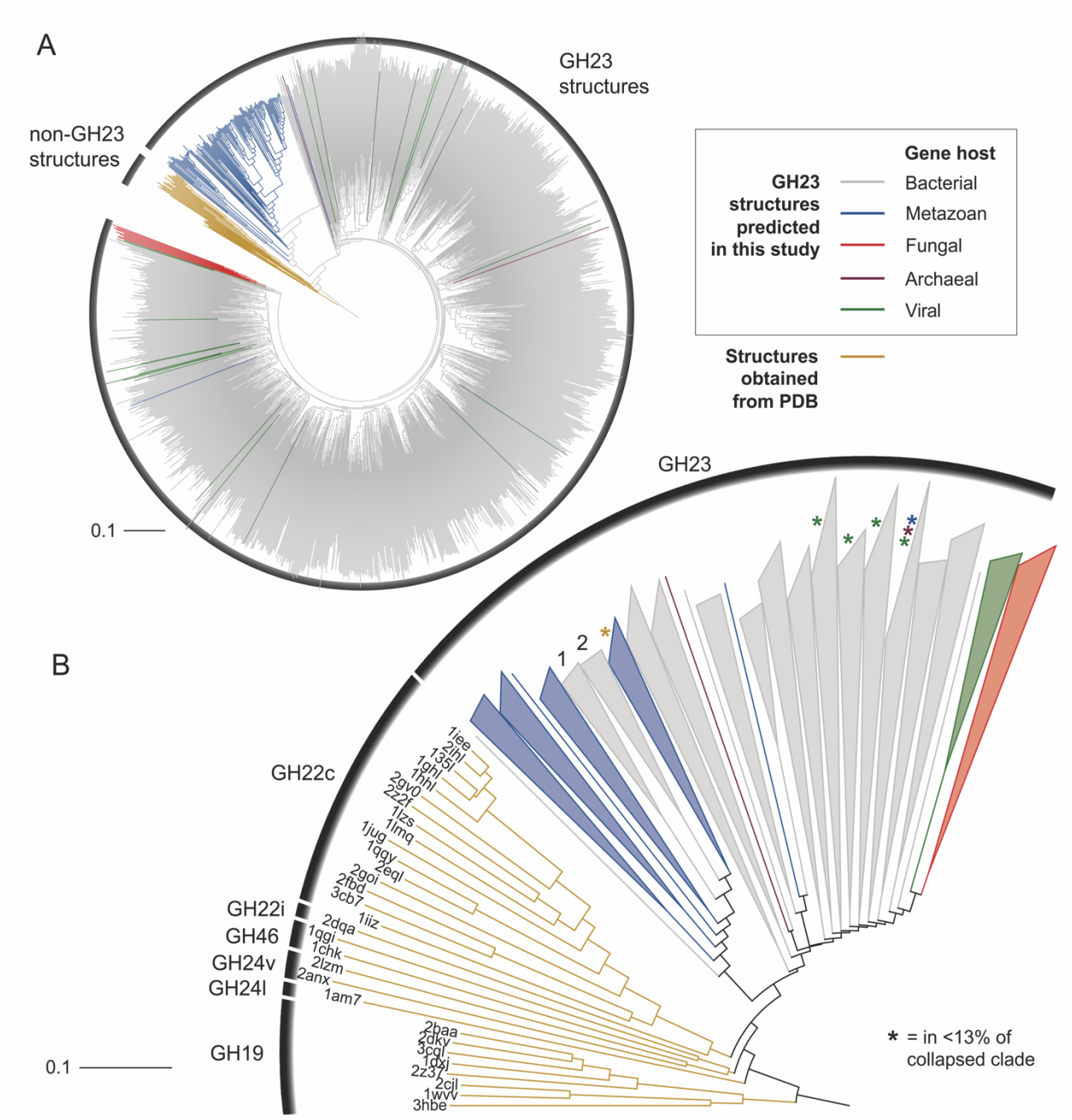

Figure 7: Structure-based phylogeny of GH families within the lysozyme superfamily. In **A**), the whole tree is depicted, in **B**), GH23 clades were collapsed and colored using the same color code as in A). Two clades of myxobacterial lysozyme clades within the metazoan GH23 clade are labeled with “1” and “2”.

413 This phylogenetic pattern is further strengthened by previous structural biology studies,
414 which showed GH23 enzymes to be more similar to the putative common molecular
415 ancestor of chitinases and murein-active glycosidases than c-type lysozymes (GH22c)
416 and i-type lysozymes (GH22i) in terms of active center organization, reaction mechanism,
417 and fold (4,37). As our sequence- and structure-based phylogenetic analyses indicate, a
418 bacterial lytic transglycosylase may have been horizontally transferred to a metazoan or
419 pre-metazoan ancestor in an ancient event and evolved into the metazoan g-type
420 lysozymes, from where a myxobacterial ancestor acquired a professional GH23
421 lysozyme gene. To reconstruct the evolutionary trajectories of lysozymes in even higher
422 detail, future genomic analyses of early-branching metazoans and metazoan-related
423 holozoans may allow to provide more comprehensive databases and to identify novel
424 glycoside hydrolase orthologues. Moreover, detailed studies on the abundance and
425 mechanisms of horizontal-gene transfer events involving eukaryotes and prokaryotes are
426 certainly needed to account for the impact of horizontal gene transfer on metazoan
427 evolution.
428
429
430
431
432
433
434
435
436
437
438
439
440
441
442

443 **Materials and Methods:**

444 ***Trichoplax* sp. H2 culture and collection**

445 Organisms of *Trichoplax* sp. H2 strain "Panama" were cultivated at room temperature in
446 petri dishes in 34 PSU filtered sea water (FSW) and fed with *Rhodomonas* sp. Water was
447 changed every two weeks and every culture was discontinued after six weeks. For
448 protein extraction, individuals were picked and transferred into clean reaction tubes with
449 FSW. After transfer of 50 to 100 individuals, the tube was shortly centrifuged to sediment
450 the animals at the bottom. Following the removal of the supernatant, the pellets were
451 stored at -20 °C until use.

452

453 ***Trichoplax* sp. H2 lysis and protein detection**

454 Sample pellets comprising 500 individuals of *Trichoplax* sp. H2 in total were lysed using
455 a total volume of 500 µL of 8 M urea, 50 mM sodium bicarbonate buffer, 300 mM NaCl,
456 pH 7.4. The pellets were suspended and pipetted up and down until the lysate appeared
457 homogenous. The lysate was centrifuged at 15,000 x *g* at 4 °C for 15 min to remove
458 insoluble debris. The supernatant was diluted with 50 mM sodium bicarbonate buffer,
459 300 mM NaCl, pH 7.4 to a final urea concentration of 1.5 M. Subsequently, the sample
460 was subjected to reversed phase fast protein liquid chromatography (FPLC) using a GE
461 ÄKTA Purifier 100 FPLC system (Amersham Biosciences). The sample was loaded on a
462 Hamilton PRP-3 microbore column and subsequently eluted in a linear gradient from
463 0.1% trifluoroacetic acid (TFA) to 80% acetonitrile (ACN) in 0.1% TFA in 20 column
464 volumes (CV). The eluate was collected in fractions of 1 mL by an autosampler. The
465 fractions were split in two aliquots each and lyophilized. One aliquot of every fraction
466 was subjected to a Western blot analysis.

467 For protein separation using Tricine-SDS-PAGE, 50 µg of extracted protein were loaded
468 onto a polyacrylamide gel consisting of a 5% stacking gel and a 13% separation gel (38).
469 The SeeBlue Plus2 protein standard (Invitrogen) was used as molecular mass reference.
470 After electrophoresis, proteins were electroblotted onto a PVDF membrane following a
471 standard semi-dry blotting protocol. Successful blotting was verified by staining with
472 Ponceau S. The membrane was washed with Tris-buffered saline (TBS) and TBS with

473 0.05% Tween 20 (TBST) and afterwards blocked using 1% bovine serum albumin (BSA)
474 in TBST. The membrane was afterwards incubated overnight with a custom polyclonal
475 antibody mix (0.88 µg/mL) against PLys, generated in two rabbits (Eurogentec). One
476 rabbit was immunized with the peptide C-TKEQQMQGGVAAYNF (Res. 239-253), the
477 other one with the peptide C-PYSSTHISQATNILI (Res. 211-225) corresponding to two
478 putatively surface-exposed alpha helices in the lysozyme domain of PLys following
479 protein structure prediction. Antibodies were enriched and purified using affinity
480 chromatography after final bleeding of the animals. After incubation with the primary
481 antibodies, the membrane was washed three times with TBST for 15 min each and
482 incubated afterwards with a monoclonal antibody against rabbit IgG coupled to
483 horseradish peroxidase (HRP) (BioCat) for 1 h. Following three washes with TBST for 15
484 min, the membrane was developed using the Amersham ECL Advanced Western
485 Blotting Detection kit (GE Healthcare) and a luminescence detector (GE Healthcare) with
486 an exposure time of 5 s. Based on the results of the Western blot, the remaining aliquots
487 of fractions containing putative proteoforms of PLys were subjected to mass
488 spectrometry.
489
490
491
492 **Top-down proteomics**
493 Lyophilized fractions from the reversed-phase FPLC fractionation (A9, A10) were
494 dissolved in 50 µL 3% acetonitrile (ACN), 0.1% trifluoroacetic acid (TFA) and centrifuged
495 at 20,000 g for 25 min at 4°C. 10 µL of the supernatant was either reduced by 5 mM
496 TCEP for 1 h at 25°C, or analyzed in its non-reduced form by LC-MS. Chromatographic
497 separation was performed on a Dionex U3000 nanoHPLC system equipped with an
498 Accucore C4 column (50 cm × 75 µm, 2.6 µm, 150 Å) coupled online to a Fusion Lumos
499 Tribrid mass spectrometer (Thermo Fisher Scientific) equipped with the High-Field-
500 Asymmetric Waveform Ion Mobility Spectrometry (FAIMS) Pro Interface. The eluents
501 used were: eluent A, 0.05% formic acid (FA); eluent B, 80% ACN, 0.04% FA. The
502 separation was performed over a programmed 90-min run. Initial chromatographic

503 conditions were 4% B for 5 min, then increased to 15% B over 2 min followed by a linear
504 gradient from 15% to 50% B over 60 min then 50 to 90% B over 2 min, and 11 min at
505 90% B. Following this, an inter-run equilibration of the column was achieved by 10
506 minutes at 4% B. A constant flow rate of 300 nl/min was employed. Wash runs were
507 performed between each sample injection. Full scan MS spectra were acquired (800-
508 1300 m/z, resolution 120,000, 4 microscans) and fragment scans of the target ions were
509 collected at CV of -15 or -10 (data dependent scans of 2, resolution 60,000) via CID
510 activation at NCE 25. Target ions were chosen after a survey scan that identified the
511 proteoform. Raw data were analyzed against a database containing a Uniprot *Trichoplax*
512 *sp. H2* proteome (13.02.2023) (12,150 sequences), Uniprot *Rhodomonas* sp. proteins
513 (374 sequences), and common contaminants (cRAP). The search was performed on
514 Proteome DiscovererTM 3.0 using a ProSightPD 4.2 search engine with a High/High
515 crawler Node (Max. RT difference 3 min and a precursor m/z tolerance of 0.5). Single
516 proteoform search node with the sequence of the proteoform was performed with a
517 precursor and fragment tolerances of 100 Da and 10 ppm, respectively.
518
519 **Bottom-up proteomics (N terminomics)**
520 Each 15 µL of the fractions 9 and 10 in 3% ACN, and 0.1% TFA were diluted to 100 µL
521 with TEAB then reduced with 10 mM DTT for 30 min at 56°C. Samples were alkylated
522 with 55 mM CAA at 25°C for 20 min in the dark. A first clean-up was performed using
523 SP3 beads (1:25 w/w protein to beads ratio) and ethanol (EtOH) added to 80% (v/v) with
524 mixing for 15 min at 25°C to induce protein binding. The supernatant was removed and
525 beads were washed three times with 80% EtOH. Dimethyl labelling (reductive
526 demethylation) of N-termini was performed by resuspending protein-bound beads in 200
527 mM HEPES (pH 7.0) and then mixing with formaldehyde (30 mM) and sodium
528 cyanoborohydride (15 mM) at 37°C for 2 h. Formaldehyde (30 mM) and sodium
529 cyanoborohydride (15 mM) was added again to each sample and kept mixing at 37°C
530 overnight. To quench the reaction, Tris buffer (pH 6.8) was added to 0.6 M for 5 h at
531 37°C. A second clean-up was done by adding EtOH to 80% for 15 min at 25°C. Then,
532 the supernatant was removed and beads were washed three times with 80% EtOH.

533 Beads were spun down to remove any remaining liquid and then reconstituted in 200
534 mM HEPES (pH 8). Digestion was performed with trypsin (1:50 enzyme to protein ratio)
535 overnight at 37 °C. Supernatant containing peptides was vacuum dried, then
536 resuspended in 3% ACN, 0.1% TFA and analyzed by LC-MS. Chromatographic
537 separation was performed on a Dionex U3000 nanoHPLC system equipped with an
538 Acclaim pepmap100 C18 column (2 µm particle size, 75 µm × 500 mm) coupled online
539 to a mass spectrometer. The same eluents as for the Top-down experiment were used.
540 The second separation was performed over a programmed 122-min run. After isocratic
541 elution at 4% B for 2 min, a linear gradient from 4% to 50% B over 90 min then 50 to
542 90% B over 5 min, and 10 min at 90% B was utilized. A constant flow rate of 300 nl/min
543 was employed. Wash runs were performed between each sample injection. Data
544 acquisition following separation was performed on a QExactive Plus (Thermo). Full scan
545 MS spectra were acquired (300-1500 m/z, resolution 70,000) and subsequent data-
546 dependent MS/MS scans were collected for the 10 most intense ions (Top10) via HCD
547 activation at NCE 27 (resolution 17,500). Dynamic exclusion (20 s duration) and a lock
548 mass (445.120025) was enabled. Raw data were analyzed against a database containing
549 a Uniprot *Trichoplax sp. H2* proteome (13.02.2023) (12,150 sequences), Uniprot
550 *Rhodomonas* sp. proteins (374 sequences) and common contaminants (cRAP). The
551 search was performed on Proteome DiscovererTM 2.5 using a SequestHT search engine
552 with 10 ppm and 0.02 Da precursor and fragment ions tolerances, respectively. Digestion
553 with Trypsin_R (semi) with a max of two missed cleavages. Oxidation (15.995 Da) of
554 methionine and dimethylation (28.031 Da) and methylation (14.016 Da) at the peptide N-
555 terminus were set as dynamic modifications. Carbamidomethylation (57.02146 Da) on
556 cysteine and dimethylation on lysine was set as a static modification. Strict parsimony
557 criteria have been applied filtering peptides and proteins at 1% false discovery rate
558 estimation.
559
560
561
562

563 **Lysoplate assay**

564 For detection of lysozyme activity, 50 *Trichoplax* sp. H2 organisms were lysed with
565 500 µL of 50 mM MES buffer, 300 mM NaCl, 1% Triton X-100, pH 5.5. Following lysis,
566 the lysate was centrifuged for at 4 °C at 12,000 x *g* for 10 min to remove insoluble debris.
567 Protein concentration was determined using a Micro BCA assay (Thermo Fisher
568 Scientific). The lysate was concentrated using 10 kDa molecular weight cut-off (MWCO)
569 ultrafiltration inlets (Merck) and 10 µL were loaded onto a lysoplate with 20 mM sodium
570 acetate, pH 5.0, into 3 mm wells (39). The raw extract was loaded onto the plate as well.
571 The lysoplate was incubated at room temperature for 24 h. Ten µL of 2 mg/mL hen egg
572 white lysozyme (Sigma-Aldrich) was used as positive control, lysis buffer as negative
573 control.

574

575 **Immunofluorescence of *Trichoplax* sp. H2**

576 *Trichoplax* sp. H2 individuals were either cryofixed using an EM ICE high pressure freezer
577 (Leica) as described previously (11) or by plunging cover slips with animals into 4%
578 paraformaldehyde (PFA) in 1.5X PHEM (PIPES, HEPES, EGTA and MgCl2) buffer, pH 7.0
579 (40). For high pressure freezing, the animals were first transferred into planchets, covered
580 with hexadecane as filler, and subsequently subjected to high pressure freezing. The
581 vitrified samples were subjected to freeze substitution using a freeze substitution (FS)
582 machine (Leica), following an adapted protocol from Mayorova et al. (16). Briefly,
583 samples were freeze substituted in acetone with 0.5% uranyl acetate at -90 °C for 8 h,
584 followed by incubation at -60 °C for 8 h and at -40 °C for 8 h. After washing with ethanol,
585 samples were progressively infiltrated with medium hardness LOWICRYL HM20 resin at
586 -40 °C (33%, 66%, 100%, each for 2 h), followed by 100% resin overnight. Samples
587 were transferred to fresh resin in 0.2 ml PCR tubes and polymerized under indirect UV-
588 radiation at -40 °C for 48 h, followed by direct UV irradiation for 12 h at room temperature
589 in a nail polish lamp. The hardened samples were remounted and sectioned using a
590 Leica UC7 ultramicrotome and a histo diamond knife (Diatome). Transverse 300 nm thin
591 sections were transferred onto water drops on glow-discharged cover slips and heated
592 until the water evaporated. For histochemical labelling, the cover slips were first blocked

593 with 0.5% fish skin gelatine (Sigma-Aldrich) in phosphate-buffered saline (PBS) for
594 30 min, followed by incubation with Rhodamine-coupled wheat germ agglutinin (WGA),
595 diluted 1:300 in blocking buffer, at room temperature in a wet chamber for three hours.
596 Subsequently, the cover slips were washed with several changes of PBS and incubated
597 in 1 µg/ml DAPI in ddH_2O, for 10 min. The cover slips were then washed in two quick
598 changes of ddH_2O. Excessive water was removed with a filter paper and the cover slips
599 were mounted onto an 8-µL drop of Mowiol (Carl Roth). The cover slips were stored for
600 one day at room temperature at a dark place to ensure hardening of Mowiol and
601 subsequently stored at 4 °C until image acquisition. For wholemount-
602 immunofluorescence, animals were transferred onto cover slips in dishes with artificial
603 sea water (ASW) and allowed to settle for three hours. Subsequently, they were plunged
604 into 4% PFA in 1.5X PHEM buffer and fixed at room temperature for one hour.
605 Afterwards, the cover slips were washed by transferring into fresh PHEM buffer and
606 animals were photobleached for one hour using a high-intensity cold white-light LED
607 (Schott, Germany). Afterwards, the samples were blocked using 0.5% fish skin gelatine
608 in PBS with 0.1% Tween-20 (PBST) for 30 minutes in a wet chamber at room
609 temperature, followed by an overnight incubation with a custom polyclonal antibody mix
610 (Eurogentec) against PLys diluted 1:10 in blocking buffer. A negative control was
611 incubated in blocking buffer only. The next day, the cover slips were washed five times
612 with blocking buffer and incubated 30 minutes with the secondary antibody (antiRabbit-
613 FITC conjugate) diluted 1:100 and WGA-Rhodamine diluted 1:200 in blocking buffer.
614 Afterwards, the cover slips were washed in five changes of PBST and incubated in 1
615 µg/mL DAPI for five minutes. Excess liquid was blotted away using a filter paper and the
616 cover slips were mounted on drops of Mowiol on slides. Imaging was conducted with an
617 LSM 900 with Airyscan confocal microscope (Carl Zeiss) using a Plan-Apochromat
618 40x/1.4 Oil DIC M27 objective and three laser excitation wavelengths (405/488/561).
619 Images were acquired in the Airyscan Multiplex mode with tiling and subsequently
620 Airyscan processed and stitched using the Zeiss ZEN v3.2 software.
621
622

623 **Recombinant protein production and purification**

624 cDNA of mPLys_M112 and pPLys, without a signal peptide predicted using SignalP v5.0,
625 was synthesized and inserted into pET-30-a(+) plasmids, codon optimized for *E. coli*
626 (BioCat) (41). The sequence of mPLys_M112 was generated from Uniprot entry B3RIZ1,
627 while the sequence of pPLys was obtained from Uniprot entry A0A369RX22. The amino
628 acid sequence of the pPLys fusion protein (pPlys-FP) was
629 MHHHHHHSSGLVPRGSGMKETAAAKFERQHMDSPDLGTDDDDKAMKSVILLSAFVAVA
630 FAALNDDCNAGQGSCQYDSQCYTGTPASGLCPYDPSNVKCCPKVGQSCKSSTGNCML
631 TTHCGGTTYSGYCPGPSSVRCCVSSSGSGGSYPTKYGDFMRINPSGASSATARQDGLS
632 YSGVAASNKLASNDYNRCLRYKSQFQSASSSTQIPVGLITAIASRESRCGGALDSNGYGD
633 HGNGYGLMQVDKRYHSLQGGPYSSTHISQATNILISSINGVANNHRSWTKEQQMQGGV
634 AAYNFGVGNVQSIGGMDIGTTGNDYSNDVVARAQWFHNNGFN. The amino acid
635 sequence of the mPLys_M112-FP was
636 MHHHHHHSSGLVPRGSGMKETAAAKFERQHMDSPDLGTDDDDKAMGRINPSGASSAT
637 ARQDGLSYSGVAASNKLASNDYNRCLRYKSQFQSASSSTQIPVGLITAIASRESRCGGAL
638 DSNGYGDHGNGYGLMQVDKRYHSLQGGPYSSTHISQATNILISSINGVANNHRSWTKEQ
639 QMQGGVAAYNFGVSNVQSIGGMDIGTTGNDYSNDVVARAQWFHNNGFN.

640 Besides the lacking N-terminal domain, mPLys_M112 differed from pPLys only in a
641 single amino acid substitution from glycine to serine in amino acid position 256. As this
642 residue is located inside a loop, oriented towards the solvent, and does not form the
643 conserved substrate binding site or active site in the predicted protein structure, we
644 considered this amino acid substitution not to affect either lysozyme activity or protein
645 stability. A chemically competent *E. coli* Shuffle *LysY* strain, which is engineered for
646 cytoplasmic expression of disulphide-bond containing proteins, was transformed with
647 the respective plasmids and grown in LB medium (50 µg/mL Kanamycin) at 37 °C and
648 150 rpm overnight. The overnight culture was split into 500 µL aliquots and mixed 1:1
649 (V/V) with glycerol. The resulting glycerol stocks were stored at -80 °C until further use.
650 Prior to recombinant protein expression, 100 mL LB medium was inoculated with 100 µL
651 glycerol stock and grown over night as described above. At the next day, 1 L TB medium
652 (50 µg/mL kanamycin) was inoculated with overnight culture to an OD600 of 0.1. When

653 the culture reached an OD600 of 0.4 to 0.6, protein expression was induced using 0.4
654 mM IPTG. For protein overexpression, the culture was incubated at 18 °C and 150 rpm
655 for 16 h. Bacteria were harvested by centrifuging at 14,500 x *g* at 4 °C for 30 min. The
656 resulting pellets were resuspended in 50 mM sodium phosphate buffer, 300 mM NaCl,
657 pH 7.4. Bacterial cells were lysed using an MS-73 sonotrode (Bandelin) following the
658 manufacturer's instructions. The lysate was cleared by centrifuging at 35,000 *x g* at 4 °C
659 for 30 min. The pellet was resuspended in buffer and the lysing and centrifuging step
660 was repeated. The resulting supernatants were collected and subjected to immobilized
661 metal-ion affinity chromatography using HiTrap Talon Crude columns with a CV of 5 mL
662 (Cytiva) and a peristaltic pump (Pharmacia). After sample loading, the column was
663 washed with 10 CV sample buffer. Overexpressed fusion protein was eluted with sample
664 buffer containing 500 mM imidazole. All further chromatographic purification steps were
665 performed on an ÄKTA Purifier FPLC. The eluted fusion proteins were desalted into a 20
666 mM Tris-HCl buffer containing 50 mM NaCl, 20 % glycerol (w/V) and 2 mM $CaCl_2$, pH
667 6.8, using a HiPrep 26/10 desalting column (Cytiva). Enterokinase, light chain (New
668 England Biolabs) was added in a ratio of 15 ng Enterokinase per milligram fusion protein.
669 After two days of incubation at room temperature, the cleaved protein of interest (POI)
670 was purified using size exclusion chromatography (SEC). For SEC, a Superdex PG 75
671 16/600 column (Cytiva) was used. After sample loading, the sample was eluted with a
672 20 mM MES buffer containing 300 mM NaCl and 20% glycerol, pH 5.5, using a flow rate
673 of 0.75 mL/min. Eluted proteins were collected in 1-mL fractions. The purified proteins
674 were snap frozen in liquid nitrogen and stored at -80 °C until use. Protein concentration
675 was determined measuring the absorbance at 280 nm and applying the calculated
676 extinction coefficient at this wavelength.
677
678 **Lysozyme assay**
679 For quantification of lysozyme activity, a turbidimetric assay after Shugar was used (42).
680 Lyophilized *Micrococcus lysodeikticus* ATCC No. 4698 (Sigma-Aldrich) (0.2 mg/mL)
681 were suspended in reaction buffer. For standard measurements a 20 mM sodium acetate
682 buffer with varying pH values was used. Different ionic strengths were adjusted with

683 NaCl. To determine the optimal pH value for lysozyme activity, a modified buffer after
684 Ellis was used, containing 5 mM sodium carbonate, 5 mM 2-amino-2-methylpropan-1,3-
685 diol, 5 mM sodium dihydrogen phosphate and 5 mM citric acid (43). For every
686 measurement, 20 µL of lysozyme solution were added to 730 µL *Micrococcus*
687 suspension. The decrease in extinction at a wavelength of 450 nm was measured
688 photometrically. For measurements at room temperature, an EasySpec UV-Vis
689 spectrophotometer (Safas) was used. Measurements at different temperatures were
690 performed with an UV2600i dual-beam absorption spectrophotometer equipped with a
691 CPS-100 temperature-controlled cuvette holder (Shimadzu). One U of lysozyme activity
692 was defined as a decrease of extinction at 450 nm of 0.001per minute (42).
693
694 **Bacterial lysis assay**
695 For assaying the lysing potential of pPLys and mPLys_M112, a membrane-
696 permeabilization assay was used, described in detail by Bruhn et al. (44). *Escherichia*
697 *coli* K12 D31 YpCr (45) and *Bacillus subtilis* (ATCC 6051) were used as target cells in this
698 assay. $1 \cdot 10^6$ CFU/well *E. coli* K12 D31 and $1 \cdot 10^5$ CFU/well in mid-logarithmic growth
699 phase were added to a dilution series of the protein of interest in a black flat-bottom 96-
700 well plate (Sarstedt), together with the DNA binding dye SYTOX Green (Invitrogen).
701 Melittin (Sigma-Aldrich) and Hen egg white lysozyme (Sigma-Aldrich) were used as
702 positive controls, protein storage buffer as negative control. pPLys and mPLys_M112
703 dilution series were measured in duplicates. Fluorescence was measured with a Tecan
704 Infinite M200 plate reader (Tecan) measuring emission at 538 nm, excited at 495 nm. If
705 possible, sigmoidal curves were fitted to the data in ORIGIN v2023 using the Boltzmann
706 function.
707
708 **Thermal shift assay**
709 Stability of recombinant mPLys_M112 and pPLys in different buffers from the Durham
710 pH Screen (Molecular Dimensions #MD1-101) was assessed by thermal shift assays (46).
711 Four µL of 5000x SYPRO Orange dye (Thermo Fisher) were added to 1 mL of protein
712 solution in 100 mM sodium phosphate, 500 mM NaCl, pH 6.5. Ten µL of this mixture

713 were distributed into a 96-well PCR plate (Sarstedt). Ten µL buffer concentrate was
714 added and the plate sealed with a transparent foil (Carl Roth). Melting curves were
715 recorded in an ABI7300 qPCR thermocycler (Thermo Fisher) through the TAMRA
716 channel. The plate was first equilibrated at 21 °C for 2 min and then the fluorescence
717 was measured for 1 min. Subsequently, the temperature was increased in 1-°C
718 increments (0.25 min equilibration followed by 1 min measurement) up to 96 °C. Curves
719 were inspected visually and then processed using *Excel* 16.69.1 (Microsoft) and *Prism*
720 9.4.1 (Graphpad) as previously described (46).
721

722 ***In situ* pH measurement of extracellular digestive events**

723 For assessment of the pH trajectory during feeding events, multiple *Trichoplax* sp. H2
724 individuales were transferred to a custom microscopic imaging chamber, filled with
725 pHRodo™-Green Zymosan particles (Thermo Fisher) in 34 PSU artificial sea water (100
726 µg/mL). Imaging was done on a Zeiss Axio Observer 7 inverted microscope with a Zeiss
727 Colibri 7 LED fluorescence source. The Zymosan particles were calibrated using buffers
728 from pH 3 to 9 (50 mM sodium phosphate, 500 mM NaCl). Quantitative imaging was
729 performed using the green fluorescence channel, 100% fluorescence intensity, 150 ms
730 exposure with a 20x Plan-Apo (NA=0.8) objective. For all pH values, the mean
731 fluorescence intensity of Zymosan particles (n=15 per pH) was assessed using Zen Blue
732 v3.9 (Zeiss) (Fig. S5-6). The same imaging settings were used for the *in situ*
733 measurements. Feeding events were followed in a time series with fluorescence and
734 brightfield micrographs every 15 s. The time series were stopped when the animals
735 interrupted feeding and started moving.
736

737 **Phylogenetic analyses of g-type lysozyme amino acid sequences**

738 The evolutionary relationships between PLys and other members of the GH23 subfamily
739 I were inferred through Maximum Likelihood (ML) phylogenetics, using the amino acid
740 alignment of the conserved g-type lysozyme domain. From the CAZY database (47), we
741 obtained the list of all 120,967 GH23 annotated proteins
742 (http://www.cazy.org/IMG/cazy_data/GH23.txt; accessed on the 1st of September

743 2023), and used the accession numbers to retrieve public sequences from the NCBI
744 protein database. The dataset was filtered to keep sequences with a length between 100
745 and 1,000 residues and that contained both the motives Glu-Ser and Glu-Leu-Met-Gln
746 that are conserved in GH23 subfamily I. Further downsampling was carried out in two
747 steps, first by randomly selecting one sequence from each host species, and then by
748 selecting one sequence per cluster at a 50% identity threshold using CD-HIT v. 4.8.1
749 (48). Additional metazoan g-type lysozyme sequences were added through rounds of
750 BLASTp searches against the non-redundant sequences database (nr) to improve the
751 representation of the group. Finally, lysozyme sequences from Porifera and Cnidaria
752 from a g-type lysozyme orthogroup (26) and myxobacterial GH23 lysozyme sequences
753 from a parallel study (27) were manually added to the dataset. A chitosanase sequence
754 from *Bacillus subtilis* was included in the dataset as outgroup (acc. num. QHE14361.1).
755 Multiple sequence alignment was carried out with Muscle v.5.1 (49) and the resulting
756 alignment was trimmed to keep residues only that aligned against the g-type lysozyme
757 conserved domain which was determined for PLys sequence through the InterProScan
758 web application (50). The ML tree of the resulting alignment was calculated with IQ-TREE
759 v.2.0.3 (51), based on the general variable time matrix (VT), a FreeRate heterogeneity
760 model with 10 categories (+R10) as selected by ModelFinder (52) and using the SH-aLRT
761 test with 1,000 bootstrap replicates for branch support. Tree representation was
762 obtained with iTOL (53). To account for the simplification generated by the
763 downsampling steps, all eukaryotic sequences removed from the initial dataset, which
764 represented 0.1% of the complete dataset, were placed in the tree following an
765 Evolutionary Placement Analysis (EPA) approach using MAFFT v.7.520 (54) to add the
766 sequences to the alignment and epa-ng v.0.3.8 (55) to build the final tree.
767

768 **Protein structure prediction and structure-based phylogenetics of the GH**
769 **lysozyme superfamily**

770 For protein structure prediction, we used ColabFold v1.5.5 which combines MMseqs2
771 with Alphafold 2, as previously described (35). Out of five generated models, we chose
772 the highest ranked model as predicted protein structure. Chimera v1.16 was used for

773 molecular visualization (56). Crystal structures of proteins from all GH families within the
774 lysozyme superfamily, following the selection used by Wohlkönig et al. (4) were obtained
775 from PDB database and included in an unrooted ML tree with the predicted protein
776 structure of PLys. The software FoldTree (36) was used to both generate pairwise
777 alignments between the three-dimensional structures and to derive an ML tree based on
778 a local structural alphabets approach.
779
780 **Author contributions**
781 HB, ML and HGV conceptualized the study. HB performed most of the experiments and
782 imaging. ID did most of the bioinformatic analysis visualized the respective data. MA and
783 AT performed the mass spectrometry experiments and analysis. MS and AS assisted
784 with the temperature stability assays and the respective analysis. UR and HB prepared
785 the samples for microscopy. HB, HGV and ML wrote the manuscript. HB designed most
786 of the figures. All authors advised the manuscript and approved the final version.
787
788 **Competing interests**
789 The authors declare that they have no competing interests.
790
791 **Data availability**
792 All proteomics raw data has been uploaded to the ProteomeXchange consortium(57) via
793 the PRIDE partner repository under the accession PXD056545 (Access for reviewers:
794 Username: reviewer_pxd056545@ebi.ac.uk, Password: GXG3RXXb2SzH). Datasets
795 used for the phylogenetic analyses can be downloaded
796 under https://doi.org/10.5281/zenodo.13889706.
797
798 .
799
800
801
802

803 **References**

804 1. McFall-Ngai M, Hadfield MG, Bosch TCG, Carey HV, Domazet-Lošo T, Douglas AE, et
805 al. Animals in a bacterial world, a new imperative for the life sciences. Proc Natl Acad Sci. 2013
806 Feb 26;110(9):3229–36.
807 2. Callewaert L, Michiels CW. Lysozymes in the animal kingdom. J Biosci. 2010
808 Mar;35(1):127–60.
809 3. Blackburn NT, Clarke AJ. Identification of Four Families of Peptidoglycan Lytic
810 Transglycosylases. J Mol Evol. 2001 Jan;52(1):78–84.
811 4. Wohlkönig A, Huet J, Looze Y, Wintjens R. Structural relationships in the lysozyme
812 superfamily: Significant evidence for glycoside hydrolase signature motifs. Uversky VN, editor.
813 PLoS ONE. 2010 Nov 9;5(11):e15388.
814 5. M. Bam,, H. Nakano. Lysozyme from placozoa, an early diverging metazoan, lyses both
815 gram-positive and negative bacteria. JSFS 85th Anniv-Commem Int Symp Symp Proc 06006
816 [Internet]. 2017; Available from: http://www.jsfs.jp/office/annual_meeting/meeting-
817 program/85th/proceeding/pdfs/06006.pdf
818 6. Najle SR, Grau-Bové X, Elek A, Navarrete C, Cianferoni D, Chiva C, et al. Stepwise
819 emergence of the neuronal gene expression program in early animal evolution. Cell. 2023
820 Oct;186(21):4676-4693.e29.
821 7. Laumer CE, Fernández R, Lemer S, Combosch D, Kocot KM, Riesgo A, et al. Revisiting
822 metazoan phylogeny with genomic sampling of all phyla. Proc R Soc B Biol Sci. 2019 Jul
823 10;286(1906):20190831.
824 8. Ringrose JH, Van Den Toorn HWP, Eitel M, Post H, Neerincx P, Schierwater B, et al.
825 Deep proteome profiling of *Trichoplax adhaerens* reveals remarkable features at the origin of
826 metazoan multicellularity. Nat Commun. 2013 Jan 29;4(1):1408.
827 9. DuBuc TQ, Ryan JF, Martindale MQ. "Dorsal–Ventral" genes are part of an ancient axial
828 patterning system: Evidence from *Trichoplax adhaerens* (Placozoa). True J, editor. Mol Biol
829 Evol. 2019 May 1;36(5):966–73.
830 10. Romanova DY, Heyland A, Sohn D, Kohn AB, Fasshauer D, Varoqueaux F, et al.
831 Glycine as a signaling molecule and chemoattractant in *Trichoplax* (Placozoa): insights into the
832 early evolution of neurotransmitters. NeuroReport. 2020 Apr 8;31(6):490–7.
833 11. Gruber-Vodicka HR, Leisch N, Kleiner M, Hinzke T, Liebeke M, McFall-Ngai M, et al.
834 Two intracellular and cell type-specific bacterial symbionts in the placozoan *Trichoplax* H2. Nat
835 Microbiol. 2019 Jun 10;4(9):1465–74.
836 12. Kamm K, Osigus HJ, Stadler PF, DeSalle R, Schierwater B. Genome analyses of a
837 placozoan rickettsial endosymbiont show a combination of mutualistic and parasitic traits. Sci
838 Rep. 2019 Nov 26;9(1):17561.
839 13. Smith CL, Varoqueaux F, Kittelmann M, Azzam RN, Cooper B, Winters CA, et al. Novel
840 cell types, neurosecretory cells, and body plan of the early-diverging metazoan *Trichoplax*
841 *adhaerens*. Curr Biol. 2014 Jul;24(14):1565–72.
842 14. Mayorova TD, Hammar K, Jung JH, Aronova MA, Zhang G, Winters CA, et al.
843 Placozoan fiber cells: mediators of innate immunity and participants in wound healing. Sci Rep.
844 2021 Dec 2;11(1):23343.
845 15. Smith CL, Pivovarova N, Reese TS. Coordinated feeding behavior in *Trichoplax*, an
846 animal without synapses. Steele RE, editor. PLOS ONE. 2015 Sep 2;10(9):e0136098.
847 16. Mayorova TD, Hammar K, Winters CA, Reese TS, Smith CL. The ventral epithelium of
848 *Trichoplax adhaerens* deploys in distinct patterns cells that secrete digestive enzymes, mucus or

849 diverse neuropeptides. Biol Open. 2019 Jan 1;bio.045674.
850 17. Kamm K, Schierwater B, DeSalle R. Innate immunity in the simplest animals –
851 placozoans. BMC Genomics. 2019 Dec;20(1):5.
852 18. Kawamura S, Ohkuma M, Chijiiwa Y, Kohno D, Nakagawa H, Hirakawa H, et al. Role
853 of disulfide bonds in goose-type lysozyme. FEBS J. 2008 Jun;275(11):2818–30.
854 19. Zavodszky M, Chen C, Huang J, Zolkiewski M, Wen L, Krishnamoorthi R. Disulfide
855 bond effects on protein stability: Designed variants of *Cucurbita maxima* trypsin inhibitor-V.
856 Protein Sci. 2001 Jan;10(1):149–60.
857 20. Daugavet MA, Shabelnikov S, Shumeev A, Shaposhnikova T, Adonin LS, Podgornaya
858 O. Features of a novel protein, rusticalin, from the ascidian *Styela rustica* reveal ancestral
859 horizontal gene transfer event. Mob DNA. 2019 Dec;10(1):4.
860 21. Daugavet MA, Shabelnikov SV, Podgornaya OI. Amino acid sequence associated with
861 bacteriophage recombination site helps to reveal genes potentially acquired through horizontal
862 gene transfer. BMC Bioinformatics. 2020 Jul;21(S12):305.
863 22. Schierwater B, Eitel M, Jakob W, Osigus HJ, Hadrys H, Dellaporta SL, et al.
864 Concatenated Analysis Sheds Light on Early Metazoan Evolution and Fuels a Modern
865 "Urmetazoon" Hypothesis. Penny D, editor. PLoS Biol. 2009 Jan 27;7(1):e1000020.
866 23. Mayorova TD, Koch TL, Kachar B, Jung JH, Reese TS, Smith CL. Placozoan secretory
867 cell types implicated in feeding, innate immunity and regulation of behavior [Internet]. 2024
868 [cited 2025 Feb 1]. Available from: http://biorxiv.org/lookup/doi/10.1101/2024.09.18.613768
869 24. McShane A, Bath J, Jaramillo AM, Ridley C, Walsh AA, Evans CM, et al. Mucus. Curr
870 Biol. 2021 Aug;31(15):R938–45.
871 25. Weston A, Vladescu SC, Reddyhoff T, Griffiths A, Crouzier T, Fielden M, et al. The
872 influence of ions on the lubricative abilities of mucin and the role of sialic acids. Colloids Surf B
873 Biointerfaces. 2023 Jul;227:113327.
874 26. Laumer CE, Gruber-Vodicka H, Hadfield MG, Pearse VB, Riesgo A, Marioni JC, et al.
875 Support for a clade of Placozoa and Cnidaria in genes with minimal compositional bias. eLife.
876 2018 Oct 30;7:e36278.
877 27. Mukherjee K, Moroz LL. Evolution of g-type lysozymes in metazoa: insights into
878 immunity and digestive adaptations. Front Cell Dev Biol. 2024 Nov 6;12:1487920.
879 28. Li Y, Zhou X, Zhang X, Xu Z, Dong H, Yu G, et al. A myxobacterial GH19 lysozyme
880 with bacteriolytic activity on both Gram-positive and negative phytopathogens. AMB Express.
881 2022 Dec;12(1):54.
882 29. Schultz DT, Haddock SHD, Bredeson JV, Green RE, Simakov O, Rokhsar DS. Ancient
883 gene linkages support ctenophores as sister to other animals. Nature. 2023 Jun 1;618(7963):110–
884 7.
885 30. Berndt H, Fuchs S, Kraus-Stojanowic I, Pees B, Gelhaus C, Leippe M. Molecular and
886 functional characterization of ILYS-5, a major invertebrate lysozyme of *Caenorhabditis elegans*.
887 Dev Comp Immunol. 2024 Oct;159:105220.
888 31. Wiens M, Korzhev M, Krasko A, Thakur NL, Perović-Ottstadt S, Breter HJ, et al. Innate
889 immune defense of the sponge *Suberites domuncula* against bacteria Involves a MyD88-
890 dependent signaling pathway. J Biol Chem. 2005 Jul;280(30):27949–59.
891 32. Illergård K, Ardell DH, Elofsson A. Structure is three to ten times more conserved than
892 sequence—A study of structural response in protein cores. Proteins Struct Funct Bioinforma.
893 2009 Nov 15;77(3):499–508.
894 33. Ingles-Prieto A, Ibarra-Molero B, Delgado-Delgado A, Perez-Jimenez R, Fernandez JM,

895 Gaucher EA, et al. Conservation of Protein Structure over Four Billion Years. Structure. 2013
896 Sep;21(9):1690–7.
897 34. Jumper J, Evans R, Pritzel A, Green T, Figurnov M, Ronneberger O, et al. Highly
898 accurate protein structure prediction with AlphaFold. Nature. 2021 Aug 26;596(7873):583–9.
899 35. Mirdita M, Schütze K, Moriwaki Y, Heo L, Ovchinnikov S, Steinegger M. ColabFold:
900 making protein folding accessible to all. Nat Methods. 2022 Jun;19(6):679–82.
901 36. Moi D, Bernard C, Steinegger M, Nevers Y, Langleib M, Dessimoz C. Structural
902 phylogenetics unravels the evolutionary diversification of communication systems in gram-
903 positive bacteria and their viruses [Internet]. 2023 [cited 2024 May 31]. Available from:
904 http://biorxiv.org/lookup/doi/10.1101/2023.09.19.558401
905 37. Monzingo AF, Marcotte EM, Hart PJ, Robertas JD. Chitinases, chitosanases, and
906 lysozymes can be divided into procaryotic and eucaryotic families sharing a conserved core. Nat
907 Struct Biol. 1996 Feb;3(2):133–40.
908 38. Schägger H, Von Jagow G. Tricine-sodium dodecyl sulfate-polyacrylamide gel
909 electrophoresis for the separation of proteins in the range from 1 to 100 kDa. Anal Biochem.
910 1987 Nov;166(2):368–79.
911 39. Osserman EF, Lawlor DP. Serum and urinary lysozyme (muramidase) in monocytic and
912 monomyelocytic leukemia. J Exp Med. 1966 Nov 1;124(5):921–52.
913 40. Montanaro J, Gruber D, Leisch N. Improved ultrastructure of marine invertebrates using
914 non-toxic buffers. PeerJ. 2016 Mar 31;4:e1860.
915 41. Almagro Armenteros JJ, Tsirigos KD, Sønderby CK, Petersen TN, Winther O, Brunak S,
916 et al. SignalP 5.0 improves signal peptide predictions using deep neural networks. Nat
917 Biotechnol. 2019 Apr;37(4):420–3.
918 42. Shugar D. The measurement of lysozyme activity and the ultra-violet inactivation of
919 lysozyme. Biochim Biophys Acta. 1952 Jan;8:302–9.
920 43. Ellis DA. A new universal buffer system. Nature. 1961 Sep;191(4793):1099–100.
921 44. Bruhn H, Riekens B, Berninghausen O, Leippe M. Amoebapores and NK-lysin, members
922 of a class of structurally distinct antimicrobial and cytolytic peptides from protozoa and
923 mammals: a comparative functional analysis. Biochem J. 2003 Nov 1;375(3):737–44.
924 45. Boman HG, Monner DA. Characterization of lipopolysaccharides from *Escherichia coli*
925 K-12 mutants. J Bacteriol. 1975 Feb;121(2):455–64.
926 46. Huynh K, Partch CL. Analysis of protein stability and ligand interactions by thermal shift
927 assay. Curr Protoc Protein Sci [Internet]. 2015 Feb [cited 2024 May 31];79(1). Available from:
928 https://currentprotocols.onlinelibrary.wiley.com/doi/10.1002/0471140864.ps2809s79
929 47. Drula E, Garron ML, Dogan S, Lombard V, Henrissat B, Terrapon N. The carbohydrate-
930 active enzyme database: functions and literature. Nucleic Acids Res. 2022 Jan 7;50(D1):D571–7.
931 48. Fu L, Niu B, Zhu Z, Wu S, Li W. CD-HIT: accelerated for clustering the next-generation
932 sequencing data. Bioinformatics. 2012 Dec 1;28(23):3150–2.
933 49. Edgar RC. Muscle5: High-accuracy alignment ensembles enable unbiased assessments of
934 sequence homology and phylogeny. Nat Commun. 2022 Nov 15;13(1):6968.
935 50. Jones P, Binns D, Chang HY, Fraser M, Li W, McAnulla C, et al. InterProScan 5:
936 genome-scale protein function classification. Bioinformatics. 2014 May 1;30(9):1236–40.
937 51. Nguyen LT, Schmidt HA, Von Haeseler A, Minh BQ. IQ-TREE: A fast and effective
938 stochastic algorithm for estimating Maximum-Likelihood phylogenies. Mol Biol Evol. 2015
939 Jan;32(1):268–74.
940 52. Kalyaanamoorthy S, Minh BQ, Wong TKF, Von Haeseler A, Jermiin LS. ModelFinder:

941 fast model selection for accurate phylogenetic estimates. Nat Methods. 2017 Jun;14(6):587–9.
942 53. Letunic I, Bork P. Interactive Tree Of Life (iTOL) v5: an online tool for phylogenetic tree
943 display and annotation. Nucleic Acids Res. 2021 Jul 2;49(W1):W293–6.
944 54. K. Kathoh, M. Frith. Adding unaligned sequences into an existing alignment using
945 MAFFT and LAST. Bioinformatics. 2012;28:3144–6.
946 55. P. Barbera, A. M. Kozlov, L. Czech, B. Morel, D. Darriba, T. Flouri, et al. EPA-ng:
947 Massively parallel evolutionary placement of genetic sequences. Syst Biol. 2019;68:365–9.
948 56. Pettersen EF, Goddard TD, Huang CC, Couch GS, Greenblatt DM, Meng EC, et al.
949 UCSF Chimera—A visualization system for exploratory research and analysis. J Comput Chem.
950 2004 Oct;25(13):1605–12.
951 57. Vizcaíno JA, Deutsch EW, Wang R, Csordas A, Reisinger F, Ríos D, et al.
952 ProteomeXchange provides globally coordinated proteomics data submission and dissemination.
953 Nat Biotechnol. 2014 Mar;32(3):223–6.
954

955 **Acknowledgements**

956 We thank Ina Kraus-Stojanowic and Antonia Stanislaus for their support during the
957 recombinant expression and characterization of pPLys, Heidrun Ließegang for
958 assistance of placozoan culturing and the Central Microscopy (CAU) for their support
959 with HPF&FS, ultramicrotomy (Ulrike Voigt and Tanja Zabel) and for providing the Zeiss
960 LSM900 confocal microscope (the German Research Foundation INST 257/650-1
961 FUGG). Part of this work was performed at the Multi-User CryoEM Facility at the Centre
962 for Structural Systems Biology, Hamburg, supported by the Universität Hamburg and
963 DFG grant numbers (INST 152/772-1|152/774-1|152/775-1|152/776-1|152/777-1
964 FUGG). We also thank Tim Laugks for technical assistance with high pressure freezing
965 and Brandon Seah for valuable suggestions on the manuscript.
966
967